Chapter 1: Cathodoluminescence Hyperspectral Imaging in Geoscience

P. R. Edwards
Department of Physics
SUPA
University of Strathclyde
107 Rottenrow
Glasgow G4 0NG, UK
paul.edwards@strath.ac.uk

M. R. Lee
School of Geographical and Earth Sciences
University of Glasgow
Gregory Building
Lilybank Gardens
Glasgow G12 8QQ, UK
Martin.Lee@Glasgow.ac.uk

INTRODUCTION

Cathodoluminescence (CL) is the electron-stimulated emission of low-energy (IR/visible/UV) photons from a solid material. Electron irradiation raises sample electrons to an excited state, which then emit a photon as they return to a lower energy state. The resultant luminescence can be analysed both *spatially* and *spectrally*, and until recently only one of these two approaches could be used for a given measurement. This chapter outlines the conventional spatial and spectral techniques, then describes the more recent approach of hyperspectral imaging, in which a single CL dataset *simultaneously* contains both spatial and spectral information.

Many different factors influence the intensity and wavelength of CL, including: (i) the band-gap energy of the mineral; (ii) the presence of structural defects (vacancies, dislocations *etc.*); and (iii) the presence and concentration of trace elements. These latter centres may introduce mid-gap states that become available for electronic transitions; alternatively they may allow intra-ion transitions such as within the *d* orbitals of transition metals (which exhibit a strong dependence on the crystal field: Fleischauer and Fleischauer 1970) or the *f* orbitals of rare earth elements (REE) (that are less sensitive to the properties of the host material). Those emission bands whose origin is independent of the presence of impurity atoms are termed ‘intrinsic’, while ‘extrinsic’ refers to the luminescence resulting from trace elements within the mineral. The concentrations of elements required to produce extrinsic CL peaks can be orders of magnitude lower than those measurable by X-ray microanalysis in energy-dispersive (EDX) or wavelength-dispersive (WDX) mode.

While some structural defects and extrinsic centres contribute luminescence bands to the emission spectrum, others act to reduce the intensity of CL. This can be due to the

introduction of nonradiative pathways via which excited electrons may relax without emitting a photon. When this process is attributed to the presence of a particular element, the phenomenon is referred to as quenching.

A variety of technologies are used to collect and analyse the photons emitted from a mineral as a consequence of electron irradiation, and they can be divided into two classes: (i) spatial (i.e. imaging) techniques that record light emitted over a certain wavelength range (here termed optical-CL and SEM-CL); (ii) spectroscopic methods that quantify emission wavelengths, typically centred on the visible range but often extending into the ultra-violet (UV) and infra-red (IR) wavelengths. The spectra may be acquired from single points or from an array; the latter is the basis of the hyperspectral techniques that are the focus of this chapter. However, in order to understand better the advantages and further potential of hyperspectral imaging in geoscience we first outline the more established methods for characterisation of CL in minerals.

Most of the examples referred to this chapter use calcite because it is one of the most intensively-studied minerals, for reasons that include: (i) it commonly has a high intensity of CL emission at visible wavelengths; (ii) its extrinsic centres and quenchers are fairly well known; (iii) calcite is commonplace in a wide range of rock types on Earth and beyond (e.g. meteorites from Mars and primitive asteroids); (iv) the precipitation and dissolution of calcite is an important determinant of the evolution of porosity and permeability in hydrocarbon reservoir rocks, and so understanding its growth history is economically significant; (v) biogenic and inorganic calcite is an important climate proxy (e.g. brachiopod shells, speleothems) and CL is used widely to screen samples for evidence of diagenetic alteration prior to chemical or isotopic analysis (Barbin 2013).

The technology and geological applications of conventional optical and SEM-based CL imaging and single point spectroscopy has been the subject of a series of reviews over the last 35 years. These include books (e.g. Marshall 1988, Pagel *et al.* 2000, Boggs & Krinsley 2006), journal special issues (e.g. *Sedimentary Geology* volume 65, issue 3/4, 1989; *Mineralogy and Petrology* volume 107, Issue 3, 2013) and review papers (e.g. Richter *et al.* 2003, Götze & Kempe 2008, 2009, Götze 2012). By contrast the applications of hyperspectral CL imaging to mineralogy and petrology are still in their infancy, and the technique has been used by only a small number of research groups (e.g. Lee *et al.* 2005, 2006, England *et al.* 2006, Edwards *et al.* 2007, Parsons *et al.* 2008, MacRae *et al.* 2012, 2013). However, hyperspectral techniques have been applied more widely in physics (e.g. Christen *et al.* 1991, Edwards & Martin 2011). Below we outline existing technologies for CL in geoscience and their applications, concentrating on optical and SEM-based methods, prior to describing the background, principles and applications of hyperspectral imaging.

OPTICAL-CL IMAGING

Instrumentation

The first studies of CL in geology used an electron microprobe (Long & Agrell 1965), but simpler and less expensive 'optical-CL' systems employing a conventional petrographic microscope were soon developed (e.g. Sippel 1965), and have remained the mainstay of CL imaging in geology. Optical-CL uses a polished thin section or block that is irradiated with

electrons within a small vacuum chamber that is mounted on the stage of a petrographic microscope. The luminescence can be viewed through the microscope eyepieces or recorded using a digital camera. The electron beam is static and defocused, and two different electron sources are available; 'cold cathode' (whereby electrons are generated from an ionised gas within a 'flood' gun) and 'hot cathode' (whereby electrons are generated from a heated filament similar to the emitter of a SEM or electron probe microanalyser (EPMA)). The cold cathode instruments have the advantage that they operate at lower vacuum ($<10^{-2}$ Torr for cold cathode against $<10^{-5}$ to 10^{-6} Torr for hot cathode) and the samples do not require a prior conductive coating (which can otherwise absorb a significant amount of the light emitted). The configuration of optical-CL systems are discussed in more detail by Marshall (1988), Remond *et al.* (2000), Boggs & Krinsley (2006), Götze & Kempe (2008) and Götze *et al.* (2013).

Despite its widespread use, there are several important limits to the capabilities of optical-CL. Firstly, spatial resolution of the images is constrained by the light collection optics, with the combination of diffraction (the wavelength limit) and lens aberrations leading to minimum feature sizes of typically a few micrometres being resolvable. Secondly, the wavelength range of luminescence that can be observed is usually limited to the visible part of the electromagnetic spectrum; this is largely due to the use of colour cameras as detectors, although these have been adapted for near-IR imaging (Barwood 2007). In addition, the description of emission wavelength and intensity is qualitative and reproducibility will depend on the spectral response of the hardware (i.e. CCD) used to record the images. Although optical-CL systems can be coupled to a spectrograph in order to determine emission wavelengths, and to EDX detectors to reveal mineral chemistry (Vortisch *et al.* 2003), spectroscopy and chemical analysis (e.g. by analytical SEM or EPMA) are both usually undertaken *ex-situ*, and re-locating areas of interest can be difficult and time consuming.

Applications

Calcite may be optically non-luminescent, or have blue or yellow/orange/red CL (hereafter referred to as 'orange' for brevity). The first optical CL images of calcite revealed intracrystalline variations in emission wavelength and/or intensity (i.e. concentric zoning; Sippel & Glover 1965), which are now known to be a ubiquitous feature of cements (**Figs 1-1; 1-2**). Chemical analysis by EPMA showed that concentric zoning reflects changes in the abundance and/or type of activators and quenchers that were incorporated during crystal growth (Long and Agrell 1965, Sippel & Glover 1965, Smith & Stenstrom 1965). Where trace elements are partitioned differently between faces of the same crystal, sector zones can be recognised (Reeder & Grams 1987). Concentric zoning reveals the habit and growth direction of crystals (**Fig. 1-1**), and discontinuities highlight corrosion surfaces. Sippel & Glover (1965) first suggested that zoning patterns could be correlated between samples, and this concept of 'cement stratigraphy' was championed by Meyers (1978). Subsequent studies have suggested that there may be a common sequence of CL zones which develop within a carbonate rock as its pores are cemented during burial (e.g. Richter *et al.* 2003) or uplift (Lee & Harwood 1989).

In the absence of trace element centres, calcite luminesces blue, which is an intrinsic emission that is related either to lattice defects (Sippel & Glover 1965, Walker *et al.* 1989) or a CO_3 centre (Calderon *et al.* 1984). Transition metal ions are the principal extrinsic determinants of calcite CL; Mn^{2+} is the main activator and Fe^{2+} is the main quencher. The concentration of Mn required to activate optically detectable CL is in the range of a few tens of ppm (e.g. Fairchild 1983, ten Have & Heijnen 1985, Mason 1987, Habermann *et al.* 1998, 2000, Budd *et al.* 2000). In the absence of Fe, CL colour changes progressively from violet/purple to orange as Mn concentrations increase towards the few tens of ppm level (Habermann *et al.* 1998, Cazenave 2003). If Fe is low (i.e. <~200 ppm) there is an approximately linear relationship between the intensity of the orange CL and Mn concentrations up to ~500–1000 ppm; at higher concentrations of Mn luminescence intensities fall owing to self-quenching (also termed 'concentration quenching') (e.g. Mason 1987, Habermann *et al.* 2000). The concentration of Fe required to quench the orange band varies with Mn values; for example where Mn is <200 ppm, quenching starts at Fe concentrations of 100 ppm (Budd *et al.* 2000), and quenching for any Mn concentration effective at >3000–4000 ppm Fe (Habermann *et al.* 2000). Other activators of CL in calcite include REE^{3+} (Mason and Mariano 1990; Habermann *et al.* 1996), although their contribution is often difficult to detect by optical-CL owing a stronger overlapping orange emission from the Mn centre.

SEM-BASED CL IMAGING

Instrumentation

SEM-based CL imaging (i.e. SEM-CL) developed soon after the cold cathode based optical systems (e.g. Krinsley & Hyde 1971). The most commonplace SEM-CL systems use a parabolic mirror to guide light that is emitted as the focused electron beam is rastered over the specimen surface to a photomultiplier. The signal from the photomultiplier is then sent to the microscope software to form an image. Typically these images are 'panchromatic', which means that they are formed from all of the light detected by the photomultipler (i.e. wavelengths are unresolved). The images therefore represent variations in CL emission intensity over the sensitivity range of the photomultiplier (and the collection system where applicable), and are formed in greyscale. More sophisticated systems have selectable filters between the sample and photomultiplier so that monochromatic images can be formed from specified wavelength ranges. These images can then be false coloured and overlain on each other to provide a 'real colour' composite image.

SEM-CL can use polished thin sections or polished blocks, which may or may not need a conductive coating depending on the capabilities and operating conditions of the SEM. Most SEMs will enable CL images to be acquired simultaneously or sequentially with secondary and backscattered electron images and EDX/WDX spot analyses or maps, thus enabling specific CL characteristics to be related to mineral chemistry and microstructure. The crystallographic orientation of features identified by CL (e.g. zone boundaries) can also be determined by electron backscatter diffraction (EBSD), although as EBSD is undertaken at a tilt of ~70º, it cannot usually be performed simultaneously with CL imaging. In contrast to optical-CL, most SEM-CL systems are not limited to visible wavelengths (i.e. there are no

glass optics that would otherwise prevent short wavelength radiation (i.e. <380 nm) from reaching the photomultiplier) and can form images over the entire sensitivity range of the photomultiplier (typically ~200–850 nm) (**Fig. 1-2**). Other advantages of SEM-CL over optical systems are: (i) its high spatial resolution, which is now limited only by the electron spot size and the beam–sample interaction volume, rather than the collection optics (e.g. can resolve sub-micrometer scale zoning; **Fig. 1-2**); and (ii) high sensitivity, due to the use of higher quantum efficiency detectors such as photomultipliers, enabling the imaging of low luminescence intensities.

SEM-CL has two principal limitations relative to optical-CL: (i) image quality can be significantly degraded by phosphorescence (i.e. the continued emission of photons following the cessation of electron stimulation; Marshall 1998), and (ii) as the photomultipliers used are sensitive to a different region of the electromagnetic spectrum to the eye/CCD, they cannot necessarily be interpreted in the same way as optical-CL images (e.g. calcite with a high emission intensity in SEM-CL would not necessarily display a bright orange luminescence in optical-CL; **Fig. 1-2**). Both of these problems are discussed below with reference to imaging of calcite.

Applications

SEM-CL has been used with great success to study a wide range of silicate minerals. For example it enables identification of multiple generations of quartz within sandstones from differences in their emission intensities (i.e. detrital quartz grains are commonly luminescent whereas the cements are almost exclusively non-luminescent; e.g. Makowitz & Milliken, 2003). SEM-CL is also a very valuable tool for revealing fine-scale growth zoning within zircon (e.g. Hay & Dempster 2009), and analysis of these zones by ion microprobe can then be used to reveal the chronology of crystal growth.

In contrast to silicates, SEM-CL imaging of calcite is hindered significantly by phosphorescence (Marshall 1988, Reed & Milliken 2003, Lee *et al.* 2005). Several solutions to this process have been proposed. The simplest is to increase the dwell time of the electron beam at each point in the raster to a value that is greater than the time taken for CL to decay from previous points (Lee 2000). The optimum dwell time therefore depends on rates of luminescence decay, which vary between emission centres. Using laser stimulation, Gaft *et al.* (1998, 2001) showed that emission from the Mn^{2+} centre in calcite has a 1.5 millisecond (ms) decay time whereas luminescence over the 400–500 nm range has sub-ms decay times. Using this information, Lee *et al.* (2005) found that the phosphorescence of Mn^{2+}-activated CL can be minimised by using a dwell time to 6.4 ms or greater, and regions of calcite with UV-blue CL can be successfully imaged using shorter dwell times. The alternative strategy for overcoming the deleterious effects of phosphorescence is to form the image using only the rapidly decaying shorter wavelength emission by placing a UV-blue filter between the sample and photomultiplier (Reed & Milliken 2003). Sharp and detailed images of zoned carbonate cements can be formed using this 'limited wavelength imaging' technique (Reed & Milliken 2003). Its advantage over the 'dwell time' approach is that high-resolution images can be formed much more rapidly (i.e. with a sub-ms dwell at each point). The disadvantages of the limited wavelength technique are that as the images are formed using only part of the light

being emitted by the sample, signal/noise ratios may be low, and in order to correctly interpret these images in terms of geological processes (e.g. changes to pore water chemistry, pH and Eh) the activators of UV-blue CL need to be understood (Lee *et al.* 2005).

SEM-CL has been used successfully to image zoning in calcite from CM2 carbonaceous chondrite meteorites (Lee & Ellen 2008), and integration with EBSD mapping can reveal changes to crystal habit during growth (**Fig. 1-3**). The technique has also been applied to terrestrial carbonate cements (Lee 2000, Reed & Milliken 2003, Lee *et al.* 2005), and as highlighted by Lee (2000), SEM-CL images contain a wealth of detail that are absent from corresponding optical-CL images (**Fig. 1-2**). This mismatch between optical-CL and SEM-CL reflects differences in the wavelength sensitivity ranges of the two techniques, and means that SEM-CL images of calcite cannot be interpreted in terms of variations in the concentrations of Mn and Fe, as can most optical-CL images. The emission that is detectable by SEM-CL but not optical-CL is at UV wavelengths, and may relate to an intrinsic centre (e.g. REE) and/or lattice defects, and these possibilities are discussed in more detail below in the light of information obtainable by hyperspectral techniques.

SINGLE POINT CL SPECTROSCOPY

In order to positively identify the centres responsible for features in CL images such as mineral grains or zones within them, it is necessary to quantify emission wavelengths using an optical spectrometer. This has traditionally been carried out on a point-by-point basis, placing the beam at a spatial position of interest and acquiring a single spectrum. The earlier work used a scanning spectrometer and a photomultiplier, but more recently CCD spectrographs have enabled faster acquisition. Irrespective of the detector used, the spectral resolution obtainable in such a measurement is a function of the entrance slit width, the focal length and the grating ruling density of the spectrometer; the optics of the light collection and spectrometer are discussed in greater depth in the next section.

The ability to acquire a quick spectrum from a sample is a useful tool, and will remain so even with the wider adoption of hyperspectral imaging. One drawback, however, is that—like monochromatic imaging—it relies on some prior knowledge of the features of interest in the sample. That is, we need to know at which spatial position to acquire a spectrum, just as we would need to know at what wavelength we should acquire a map. Even combining optical-CL or SEM-CL with single point spectroscopy can lead to spectral or spatial features of interest being missed.

CL HYPERSPECTRAL IMAGING

The extension of SEM-based CL into the hyperspectral imaging (HSI) domain brings a number of significant advantages compared with the conventional imaging and spectroscopy variants of the technique. At the same time, this method of data acquisition also presents a number of new challenges, particularly in the areas of optical design and data analysis.

Background to hyperspectral imaging

'Hyperspectral image' is the term given to a dataset containing both spatially- and spectrally-resolved information. It can be considered as a two-dimensional array of spectra, or—

equivalently—as an aligned stack of monochromatic images. **Figure 1-4** is a conceptual representation of this 'data cube'. The term *hyperspectral* is borrowed from its original use in the field of remote sensing: when colour aerial or satellite images began to be supplemented with a small number of additional images from discrete, non-visible wavelength bands, this was referred to as *multispectral* imaging; the term *hyperspectral* was then coined to differentiate the case in which a large number of contiguous bands (typically >20) are simultaneously imaged (van der Meer *et al.* 2012).

Such hyperspectral reflectance measurements now have many applications beyond remote sensing, with the technique being widely used, for example, in forensics (Edelman *et al.* 2012) and food production (Qin *et al.* 2013). Several electron microscopy/spectroscopy signals also lend themselves to HSI, including, for example: EDX; electron energy loss spectroscopy (EELS); and CL.

Christen *et al.* (1991) introduced CL-HSI (or 'spectrum mapping') in the analysis of optoelectronic semiconducting materials. It is now widely used in this field, with a particular strength being the ability to map shifts in emission peak wavelength due to spatial variations in properties such as elastic strain, alloy composition, electric field or temperature. While this specific feature is less useful when looking at minerals, there are still a number of advantages to the technique which have resulted in its yet modest but increasing use in geoscience.

Advantages of hyperspectral imaging

The most obvious benefit of measuring CL in hyperspectral mode is simply that more data is acquired in a single measurement. Even if a hyperspectral image is considered to be nothing more than a large number of discrete monochromatic maps of the sample (which would be to disregard much of the power of the technique), the negligible costs of data storage mean that it now makes sense to measure in this mode in almost every case. Related to this benefit is the significant advantage that no prior knowledge is required concerning the spatial or spectral features in the emitted CL. There may, for example, be small inclusions within the mineral that are the only areas that luminesce at a particular wavelength. Both monochromatic imaging and point-wise spectroscopy would most likely miss these features, whereas hyperspectral CL can be used to capture all this information for later *ex-situ* data mining.

A further benefit of the hyperspectral imaging mode is the ability to deconvolve spectral features, allowing the mapping of the intensity of overlapping peaks, or separating peaks from backgrounds. Such deconvolution can be achieved through either peak fitting or the use of multivariate statistical analysis methods, as we will discuss later. Finally, one further aspect of hyperspectral imaging that differentiates it from panchromatic and monochromatic mapping is the necessary reduction in mapping speed. This is due to the data readout rates of array detectors, which typically limit spectral acquisition frequencies to ≈100 spectra/s or slower. However the mapping speed limitation need not necessarily be a disadvantage; indeed in many cases a slow scan rate may be desirable, for example: (i) when X-ray fluorescence (EDX/WDX) data are being obtained simultaneously with the CL so that acquiring a sufficient X-ray count is the rate-limiting consideration; and (ii) when dealing with a phosphorescent centre (e.g. the Mn^{2+} centre in calcite) whose CL emission decays over

ms timescales. In both these cases it makes sense to take full benefit of the imposed slow speed to acquire more CL data without additional time overhead (e.g. **Fig. 1-5**). However, it is important to consider the effect on the material of the high electron dose associated with slow scanning; for example, the linearity of the emission with varying beam current can be checked to ensure that the electron irradiation is not altering the observed CL (England *et al.* 2006).

Data acquisition

Since SEM images are, by definition, formed on a pixel-by-pixel basis, the acquisition of CL hyperspectral images is generally undertaken one spectrum at a time. (Note that this is in contrast with the majority of HSI applications outside of scanning microscopy, in which either frame-by-frame or "push-broom" methods are a more time-efficient method of building up the data cube.) In principle, this means that any CL spectroscopy setup incorporated into an SEM should be capable of acquiring a hyperspectral image. However, depending on the instrument being used for the measurement there may be additional considerations in the design of the light-collecting optics for acquiring hyperspectral images.

CL-HSI in general-purpose SEMs. Spectroscopic CL systems in SEMs require a system of optics to collect some of the light emitted from the sample and direct it towards the spectrometer for analysis and recording. Various designs of light collector have been used, with those intercepting the greatest solid angle of emitted light being based on conic sections such as ellipsoidal (Carlsson & van Essen 1974) and paraboloidal (Wright 1991) mirrors. Such arrangements are highly efficient at focusing light from a point source (the beam–sample interaction volume) to another point (the spectrometer entrance slit), making them ideal for single-point CL spectroscopy.

Moving from spectroscopy to hyperspectral imaging applies an additional constraint in that the collection efficiency now has to be maintained over an extended spatial area. The concept of *étendue* must now be considered: the product of the area of each object/image in the optical system and the solid angle of the rays forming that image remains a constant through an optical system (Lerner & Thevenon 1991). In other words, focusing the collected light to a smaller image inevitably increases the solid angle of the rays forming that image. In a CL system with a scanning beam, the object size is the sample field of view, and the image size is limited by the spectrometer entrance slit which in turn dictates the spectral resolution. The solid angle at the object defines the luminescence collection efficiency, while that at the image is fixed by the acceptance angle (*f*-number) of the spectrometer. The effect of étendue in linking these variables is therefore to impose a trade-off between the spectral resolution, field of view and collection efficiency of the optics (Yacobi & Holt 1990). As an example of the practical limitation this imposes, if the emitted CL is coupled to an *f*/4 spectrometer with a 25 μm entrance slit (chosen to match the pixel size on a 1000-channel, 1-inch array), a 10 μm field of view would limit the light collection to no more than 10% (Edwards & Martin 2011). **Figure 1-6** shows optical ray diagrams which schematically illustrate this trade-off; while this is a highly simplified picture, the same principle will apply to any light-collection arrangement (e.g. paraboloidal, ellipsoidal, fibre-coupled etc.).

CL-HSI in electron microprobes. EPMAs are dedicated scanning electron beam instruments specialized for the acquisition of WDX data. For this reason they usually contain an optical microscope built into the electron column to allow optimal positioning of the sample at the focal point of the WDX spectrometers. These built-in optics provide a ready means of collecting the emitted luminescence, and several research groups have adapted this optical pathway to allow acquisition of CL-HSIs, using both Cameca (Edwards *et al.* 2003) and JEOL (MacRae *et al.* 2012) microprobes.

Besides the convenient optics, such setups have a number of advantages over general-purpose SEM-based CL-HSI instruments. Firstly, the requirements for stimulating CL are similar to those for X-ray fluorescence generation: an electron beam current which is (i) controllable; (ii) quantifiable; (iii) potentially large (up to tens or hundreds of nanoamperes); and (iv) stable over time periods up to many hours. Secondly, they allow the simultaneous acquisition of luminescence and high-sensitivity composition data by combining CL and WDX (and EDX if also available). Finally, these instruments are designed for mapping large areas of samples, and so have high-precision scanning stages. Scanning the stage (rather than the electron beam) allows a field of view that is limited on only by the stage travel, and bypasses the problem of optical étendue encountered with a scanning beam. As an example, the dataset in **Figure 1-5** was obtained from a Cameca SX100 EPMA, and X-rays with wavelengths corresponding to several elements, including Mn and Fe, were obtained simultaneously with the CL spectra (Lee *et al.* 2005). The maps for various wavelength bands can be compared directly with counts for trace elements, enabling a qualitative correlation between the two (e.g. there is a close correspondence between the intensity of the orange peak (**Fig. 1-5b, c**) with Mn counts (**Fig. 1-5g**)). However the data can also be cross-correlated mathematically, and in the case of **Figure 1-5**, this exercise reveals a strong statistical correspondence between the intensity of the 580–650 nm wavelength band and X-ray counts on the Mn peak (**Fig. 1-5i**), and an inverse relationship with Fe (**Fig. 1-5j**), which is consistent with the 580–650 nm peak being activated by Mn and quenched by Fe.

Data analysis

The number of spectral channels in an HSI dataset is often very large, with current spectroscopic CCD arrays typically having over 1000 channels. This number will generally far exceed the actual number of underlying spectral features in the measured emission. The analysis of HSIs requires some method of reducing the raw data into a more readily digestible form in order to extract the required information.

Image slices. The simplest way of extracting 2-D images from the multi-dimensional dataset is to take 'slices' through the data cube corresponding to a range of wavelengths. This is achieved by integrating the spectrum between two wavelength limits, and repeating for each spatial pixel. This effectively generates monochromatic images from the hyperspectral image, but with the advantages over conventional monochromatic imaging that the exact centre wavelength and bandpass can be finely tuned after data acquisition, and that multiple images can be extracted from the same dataset. For example, **Figure 1-5** shows a series of images

that have been extracted from a dataset acquired from a zoned calcite cement. By forming images from different wavelength ranges, or one wavelength range subtracted from another, different zoning patterns are revealed that are a rich source of information on the distribution of various activators. The data in **Figure 1-5** are particularly important for interpreting SEM-CL images because they show that intensity variations in the UV-blue range (to which SEM-CL is most sensitive) (**Fig. 1-5e**) do not correlate with the orange band (**Fig. 1-5b, c**). Other parameters extracted from the spectra can also be mapped: for example, peak or centroid wavelengths, peak widths, maximum intensity, *etc*. It is also possible to reconstruct a 'real' colour image—using tabulated values of the response curve of the eye—for comparison with data acquired using optical-CL and colour SEM-CL systems.

Peak fitting. The above method is effective when isolated peaks are to be mapped, but is more challenging when spectrally-overlapping peaks are present. These can instead be deconvolved by fitting to peak functions: depending on the underlying energy-broadening mechanisms involved, these can include (as viewed in energy rather than wavelength space) Lorentzian, Gaussian or Voigt profiles. Non-linear least-squares minimisation algorithms are used to simultaneously fit multiple peaks to each spectrum in turn in the hyperspectral image. This method is particularly effective when mapping small changes in peak energy or width, as often encountered in semiconducting materials (*e.g.* Edwards *et al.* 2012). It is a computationally intensive method when all peak parameters (height, centre and width) are fitted, but for peaks at well-defined energies fitting time can be significantly reduced by fixing the peak positions and widths and varying only the intensities. This has been the approach taken by MacRae *et al.* (2009, 2012, 2013) in their work on converting peak intensities in hyperspectral CL to quantitative concentrations of trace-level REEs. An example of this fitting method is shown in **Figure 1-7**, which shows data acquired from a Holocene speleothem. In this case the 300–400 nm emission band is seen to be asymmetric, with shoulders on the short wavelength side of the peak. Calculating the mean of all the individual spectra and fitting to this indicated that the data in this region was well described by the sum of three Gaussian peaks centred at 368 nm, 345 nm and 299 nm. These are then fitted to each of the spectra in the hyperspectral image, holding the peak positions and widths constant and varying only the intensity to produce three images of the different components. Results from this analysis are particularly informative about the growth history of the speleothem and the contributions of different centres to the net CL signal (as expressed by the 'panchromatic' image in **Figure 1-7e**). As CL emission intensities for the 368 nm and 345 nm bands are uniform over the mapped area, they are attributed to one of more intrinsic (defect) centres. The fine-scale banding revealed in the 299 nm map is indicative of an extrinsic centre, with trace element incorporation regularly fluctuation during speleothem growth, perhaps in response to seasonal changes in solution composition. The activator of the 299 nm band is probably a REE, and possibly Ce^{3+}.

Principal component analysis. While least-squares fitting is an effective approach to mapping out peak parameters, it relies on these peaks being manually identified beforehand. Other techniques—known as multivariate statistical analysis methods—make use of the

multidimensional nature of the dataset in order to identify underlying patterns within it. Such methods are well-established in remote sensing HSI applications (van der Meer *et al.* 2012) and have also been applied to microscopy data (Kotula *et al.* 2003).

One such technique is principal component analysis (PCA), which aims to identify those components of the dataset that: (i) have the greatest *variance* (meaning that they account for the greatest fraction of the variation within the total dataset), and (ii) show the least *co-variance* (that is, they are suitably different from the other components). Mathematically, this is achieved by constructing an $n \times n$ matrix from the mean-adjusted data (where n is the number of spectral channels in the hyperspectral image) whose diagonal elements a_{ii} are the variance of the i^{th} channel and the non-diagonal elements a_{ij} are the co-variance of channels i and j. The eigenvectors of this matrix are then calculated, with these providing a new set of spectra with which to describe the dataset. In other words, while the original data is described by n monochromatic wavelengths each with an associated (monochromatic) image, the final data is described by n spectra, again each with an associated image, but now ranked by the fraction of the total variance of the dataset accounted for by each spectrum. This allows the less significant spectra (or *components*) to be disregarded, and the remaining (*principal*) components to be retained. Once the required number of components has been selected, it is usually beneficial to apply an orthogonal rotation to these, such as the varimax rotation which acts to minimise the spectral overlap between the remaining spectra (e.g. Edwards *et al.* 2012).

Figure 1-3 shows an example of applying PCA to hyperspectral image data acquired from a zoned calcite crystal in a carbonaceous chondrite meteorite. In this case, a near-UV (300–400 nm) band has been separated into two components: one correlating with a shorter wavelength peak at 270 nm, and the other correlating with a longer wavelength (~500 nm) feature. A third peak shows the Mn^{2+}-related red emission. Essentially all of the contrast in the panchromatic SEM-CL image of the crystal (**Fig. 1-3b**) relates to principal component 1, whereas the PCA technique has identified additional peaks corresponding to spatially-localised emission.

The PCA technique also makes it possible to identify and map spectral features in hyperspectral image data with extremely poor signal:noise ratios (e.g. Edwards *et al.* 2011). Because it is dependent on statistical correlations between the intensities of the different spectral channels, it is able to extract peaks that may not be visible on the individual constituent spectra.

Future developments in CL hyperspectral imaging

Hyperspectral imaging in optical-CL. There is no fundamental reason why optical-CL systems cannot be adapted to allow data acquisition in hyperspectral imaging mode, by the addition of a spectral imaging camera to the existing optics. Such cameras are commercially available, but they are mostly designed to operate in the push-broom mode—that is, one spatial line at a time, with the luminescence spectrally dispersed across the second dimension of the CCD detector array. While this arrangement is suitable when the detector and target are moving with respect to each other (such as a under a remote sensing flight-path, or with a moving production line), these would be harder to integrate into a static system such as a CL

microscope. However, recent developments have been made in the field of 'single shot' hyperspectral cameras (*e.g.* Content *et al.* 2013) which promise to produce an inexpensive method of acquiring an entire hyperspectral image on a single CCD image plane. Coupling this with an optical-CL microscope would produce a simple low-cost CL hyperspectral imaging system which—while still limited to a spatial resolution of around a micrometre by the optics—would make the technique much more widely accessible than SEM-based variants.

Time-resolved hyperspectral CL. A further tool in allowing separation of overlapping spectral peaks is to consider the relative emission decay lifetimes of different centres. If peaks from different activators are at the same wavelength but decay at different rates, the signals can be separated to varying degrees by pulsing the excitation source and measuring over an appropriately-chosen time window. This is currently achieved using time-resolved photoluminescence (PL) spectroscopy (Gaft *et al.* 1998), in which a short laser pulse is used as the excitation source. Using this approach with cathodoluminescence will benefit from the superior spatial resolution of CL over PL, and the technique could readily be extended to allow imaging.

Time-resolved CL is already widely used for investigating carrier dynamics in semiconducting materials. For example, recent developments using a femtosecond laser-pumped photocathode as an electron source allow electron beam pulses as short as picoseconds (Merano *et al.* 2005), but the longer decay times typical of luminescence from most minerals would allow a simpler electrostatic beam blanker to be used to give microsecond pulses. The ability to gate the detection windows of image-intensified CCD cameras with nanosecond resolution would allow existing hyperspectral CL setups to be adapted for TRCL with minimal alteration.

CONCLUSIONS

It is nearly 50 years since the ability of CL to provide new and powerful insights into the genesis of rocks minerals was first demonstrated. It was also at this time that optical-CL was conceived and developed, and it has remained the workhorse technique for geoscientists because it enables easy and rapid determination of both *spatial* and (qualitative) *spectral* CL properties. Here we have highlighted various aspects of the configuration and application of SEM- and EPMA-based CL technologies, and demonstrated their utility with regards to carbonates, which owing to phosphorescence have been some of the most challenging rock-forming minerals to study. The ability of hyperspectral imaging to yield *spatial* and (quantitative) *spectral* CL is set to revolutionise the way that geoscientists undertake CL, as it will enable a step-change in capability to identify and discriminate between the constituent emission bands of a CL signal, and also to identify the centres responsible. Using advanced data mining methods to fully exploit the huge depth of information contained within hyperspectral image datasets, it will possible to map ever more subtle spatial variations within the luminescence signal and to more accurately probe correlations between emission peaks from a sample.

ACKNOWLEDGEMENTS

ML acknowledges support from the UK Science and Technology Facilities Council (STFC), and PE acknowledges the support of the UK Engineering and Physical Sciences Research Council (EPSRC).

REFERENCES

BARBIN, V. (2013): Application of cathodoluminescence microscopy to recent and past biological materials: a decade of progress. *Mineralogy and Petrology* **107**, 353–362.

BARWOOD, H. (2007): Digital near-infrared (NIR) cathodoluminescence (CL) imaging and image processing. *American Mineralogist* **92**, 261–266.

BOGGS, S. JR. & KRINSLEY, D. (2006): Application of cathodoluminescence imaging to the study of sedimentary rocks. Cambridge University Press.

BUDD, D.A., HAMMES, U. & WARD, W.B. (2000): Cathodoluminescence in calcite cements: New insights on Pb and Zn sensitizing, Mn activation, and Fe quenching at low trace-element concentrations. *Journal of Sedimentary Research* **70**, 217–226.

CAZENAVE, S., CHAPOULIE, R. & VILLENEUVE, G. (2003): Cathodoluminescence of synthetic and natural calcite: the effects of manganese and iron on orange emission. *Mineralogy and Petrology* **78**, 243–253.

CALDERÓN, T., AGUILAR, M., JAQUE, F. & CY-YLL, R. (1984): Thermoluminescence from natural calcites. *Journal of Physics C: Solid State Physics* **17**, 2027–2038.

CARLSSON, L. & VAN ESSEN, C.G. (1974): An efficient apparatus for studying cathodoluminescence in the scanning electron microscope. *Journal of Physics E: Scientific Instruments* **7**, 98.

CHRISTEN, J., GRUNDMANN, M. & BIMBERG, D. (1991): Scanning cathodoluminescence microscopy—a unique approach to atomic-scale characterization of heterointerfaces and imaging of semiconductor inhomogeneities. *Journal of Vacuum Science and Technology B* **9**, 2358–2368.

CONTENT, R., BLAKE, S., DUNLOP, C., NANDI, D., SHARPLES, R., TALBOT, G., SHANKS, T., DONOGHUE, D., GALIATSATOS, N. & LUKE, P. (2013): New Microslice Technology for Hyperspectral Imaging. *Remote Sensing* **5**, 1204–1219.

EDELMAN, G., GASTON, E., VAN LEEUWEN, T., CULLEN, P. & AALDERS, M. (2012): Hyperspectral imaging for non-contact analysis of forensic traces. *Forensic Science International* **223**, 28–39.

EDWARDS, P.R. & MARTIN, R.W. (2011): Cathodoluminescence nano-characterization of semiconductors. *Semiconductor Science and Technology* **26**, 064005.

EDWARDS, P.R., MARTIN, R.W., O'DONNELL, K.P. & WATSON, I.M. (2003): Simultaneous composition mapping and hyperspectral cathodoluminescence imaging of InGaN epilayers. *Physica Status Solidi C* **0**, 2474–2477.

EDWARDS, P.R., MARTIN, R.W. & LEE, M. R. (2007): Combined cathodoluminescence hyperspectral imaging and wavelength dispersive X-ray analysis of minerals. *American Mineralogist* **92**, 235–242.

EDWARDS, P.R., SLEITH, D., WARK, A.W. & MARTIN, R. W. (2011): Mapping localized surface plasmons within silver nanocubes using cathodoluminescence hyperspectral imaging. *Journal of Physical Chemistry C* **115**, 14031–14035.

EDWARDS, P.R., JAGADAMMA, L.K., BRUCKBAUER, J., LIU, C., SHIELDS, P., ALLSOPP, D., WANG, T. & MARTIN, R. W. (2012): High-resolution cathodoluminescence hyperspectral imaging of nitride nanostructures. *Microscopy and Microanalysis* **18**, 1212–1219.

ENGLAND, J., CUSACK, M., PATERSON, N.W., EDWARDS, P., LEE, M.R. & MARTIN, R. (2006): Hyperspectral cathodoluminescence imaging of modern and fossil carbonate shells. *Journal of Geophysical Research* **111**, G03001.

FAIRCHILD, I. (1983): Chemical controls of cathodoluminescence of natural dolomites and calcites: new data and review. *Sedimentology* **30**, 579–584.

FLEISCHAUER, P.D. & FLEISCHAUER, P. (1970): Photoluminescence of transition metal coordination compounds. *Chemical Reviews* **70**, 199–230.

GAFT, M., REISFELD, R., PANCZER, G., BLANK, PH. & BOULON, G. (1998): Laser-induced time-resolved luminescence of minerals. *Spectrochimica Acta* **54**, 2163–2175.

GAFT, M., PANCZER, G., REISFELD, R. & USPENSKY, E. (2001): Laser-induced time-resolved luminescence as a tool for rare-earth element identification in minerals. *Physics and Chemistry of Minerals* **28**, 347–363.

GÖTZE, J. (2012): Application of cathodoluminescence microscopy and spectroscopy in geosciences. *Microscopy and Microanalysis* **18**, 1270–1284.

GÖTZE, J. & KEMPE, U. (2008): A comparison of optical microscope (OM) and scanning electron microscope (SEM) based cathodoluminescence (CL) imaging and spectroscopy applied to geosciences. *Mineral Mag.* **72**, 909–924.

GÖTZE, J. & KEMPE, U. (2009): Physical principles of cathodoluminescence (CL) and its applications in geosciences. In A. Gucik (ed) *Cathodoluminescence and its application in planetary science*, Springer-Verlag Berlin, pp 1–22.

GÖTZE, J., SCHERTL, H-P., NEUSER, R.D., KEMPE, U. & HANCHAR, J.M. (2013): Optical-microscope cathodoluminescence (OM-CL) imaging as a powerful tool to reveal internal textures of minerals. *Miner. Petrol.* **107**, 373–392.

HABERMANN, D., NEUSER, R.D. & RICHTER, D.K. (1996): REE-activated cathodoluminescence of calcite and dolomite: High-resolution spectrometric analysis of CL emission (HRS-CL). *Sedimentary Geology* **101**, 1–7.

HABERMANN, D., NEUSER, R.D. & RICHTER, D.K. (1998): Low limit of Mn^{2+}-activated cathodoluminescence of calcite: state of the art. *Sedimentary Geology* **116**, 13–24.

HABERMANN, D., NEUSER, R.D. & RICHTER, D.K. (2000): Quantitative high resolution spectral analysis of Mn^{2+} in sedimentary calcite. In: Pagel M *et al.* (eds) Cathodoluminescence in geosciences. Springer, Berlin Heidelberg New York Tokyo, pp 331–358.

HABERMANN, D., NIKLAS, J.R., MEIJER, J., STEPHAN, A. & GÖTTE, T. (2001): Structural point defects in "Iceland spar" calcite: *Nuclear Instruments and Methods in Physics Research B* **181**, 563–569.

HAY, D.C. & DEMPSTER, T.J. (2009): Zircon behaviour during low temperature metamorphism. *Journal of Petrology* **50**, 571–598.

KOTULA, P.G., KEENAN, M.R. & MICHAEL, J.R. (2003): Automated analysis of SEM X-ray spectral images: a powerful new microanalysis tool. *Microscopy and Microanalysis* **9**, 1–17.

KRINSLEY, D.H. AND HYDE, P. (1971): Cathodoluminescence studies of sediments. Scanning Electron Microscopy, Proceedings of 8th Annual SEM Symposium, IITRI, Chicago, pp. 409–416.

LEE, M.R. (2000): Imaging of calcite by optical and SEM cathodoluminescence. *Microscopy and Analysis* **70**, 15–16.

LEE, M.R. & HARWOOD, G.M. (1989): Dolomite calcitization and cement zonation related to uplift of the Raisby Formation (Zechstein carbonate), northeast England. *Sedimentary Geology* **65**, 285–305.

LEE, M.R. & ELLEN, R. (2008): Aragonite in the Murray (CM2) carbonaceous chondrite: implications for parent body compaction and aqueous alteration. *Meteoritics and Planetary Science* **43**, 1219–1231.

LEE, M.R., MARTIN, R.W., TRAGER-COWAN, C. & EDWARDS, P.R. (2005): Imaging of cathodoluminescence zoning in calcite by scanning electron microscopy and hyperspectral mapping. *Journal of Sedimentary Research* **75**, 313–322.

LEE, M.R., PARSONS, I., EDWARDS, P.R. & MARTIN, R.W. (2006): Identification of cathodoluminescence activators in zoned alkali feldspars by hyperspectral imaging and electron probe microanalysis. *American Mineralogist* **92**, 243–253.

LERNER, J. & THEVENON, A. (1991): The Optics of Spectroscopy—A tutorial. Jobin Yvon.

LONG, J.V.P & AGRELL, S.O. (1965): The cathodo-luminescence of minerals in thin section. *Mineralogical Magazine* **34**, 318–326.

MACRAE, C.M., WILSON, N.C. & BRUGGER, J. (2009): Quantitative cathodoluminescence mapping with application to a Kalgoorlie scheelite. *Microscopy and Microanalysis* **15**, 222–230.

MACRAE, C.M., WILSON, N.C., TORPY, A. & DAVIDSON, C.J. (2012): Hyperspectral cathodoluminescence imaging and analysis extending from ultraviolet to near infrared. *Microscopy and Microanalysis* **18**, 1239–1245.

MACRAE, C.M., WILSON, N.C. & TORPY, A. (2013): Hyperspectral cathodoluminescence. *Mineralogy and Petrology* **107**, 429–440.

MAKOWITZ, A. & MILLIKEN, K.L. (2003): Quantification of brittle deformation in burial compaction, Frio and Mount Simon Formation sandstones. *Journal of Sedimentary Research* **73**, 1007–1021.

MARSHALL, D.J. (1988): Cathodoluminescence of Geological Materials: Boston, Unwin-Hyman, 146 p.

MASON, R.A. (1987): Ion microprobe analysis of trace elements in calcite with an application to the cathodoluminescence zonation of limestone cements from the Lower Carboniferous of South Wales, U.K. *Chemical Geology* **64**, 209–224.

MASON, R.A. & MARIANO, A.N. (1990): Cathodoluminescence activation in manganese-bearing and rare earth–bearing synthetic calcites. *Chemical Geology* **88**, 191–206.

MERANO, M., COLLIN, S., RENUCCI, P., GATRI, M. SONDEREGGER, S., CROTTINI, A., GANIÈRE, J.-D. & DEVEAUD, B. (2005): High brightness picosecond electron gun. *Review of Scientific Instruments* **76**, 085108.

MEYERS, W.J. (1978): Carbonate cements—their regional distribution and interpretation in Mississippian limestones of southeastern New Mexico. *Sedimentology* **25**, 371–400.

PAGEL, M., BARBIN, V., BLANC, P. & OHNENSTETTER, D. (eds) (2000): Cathodoluminescence in geosciences. Springer, Berlin Heidelberg New York Tokyo, 514 pp.

PARSONS, I., STEELE, D.A., LEE, M.R. & MAGEE, C.W. (2008): Titanium as a cathodoluminescence activator in alkali feldspars. *American Mineralogist* **93**, 875–879.

QIN, J., CHAO, K., KIM, M.S., LU, R. & BURKS, T.F. (2013): Hyperspectral and multispectral imaging for evaluating food safety and quality. *Journal of Food Engineering* **118**, 157–171.

REED, R.M. & MILLIKEN, K.L. (2003): How to overcome imaging problems associated with carbonate minerals on SEM-based cathodoluminesence systems. *Journal of Sedimentary Research* **73**, 328–332.

REEDER, R.J. & GRAMS, J.C. (1987): Sector zoning in calcite cement crystals—implications for trace-element distributions in carbonates. *Geochimica et Cosmochimica Acta* **51**, 187–194.

REMOND, G., PHILLIPS, M.R. & ROQUES-CARMES, C. (2000): Importance of instrumental and experimental factors on the interpretation of cathodoluminescence data from wide band gap materials. in PAGEL M, BARBIN V, BLANC P, OHNENSTETTER D (eds) (2000) Cathodoluminescence in geosciences. Springer, Berlin Heidelberg New York Tokyo, 59–126.

RICHTER, D.K., GÖTTE, TH, GÖTZE, J. & NEUSER, R.D. (2003): Progress in application of cathodoluminescence to sedimentary petrology. *Mineralogy and Petrology* **79**, 127–166.

SIPPEL, R.F. (1965): Simple device for luminescence petrography. *Rev. Scient. Instr.* **36**, 556–558.

SIPPEL, R.F. & GLOVER, E.D. (1965): Structures in carbonate rocks made visible by luminescence petrography. *Science* **150**, 1283–1287.

SMITH, J.V. & STENSTROM, R.C. (1965): Electron-excited luminescence as a petrolgic tool. *Journal of Geology* **73**, 627–635.

TEN HAVE, T. & HEIJNEN, W. (1985): Cathodoluminescence activation and zonantion in carbonate rocks: an experimental approach. *Geologie en Mijnbouw* **64**, 297–310.

VAN DER MEER, F.D., VAN DER WERFF, H.M., VAN RUITENBEEK, F.J., HECKER, C.A., BAKKER, W.H., NOOMEN, M.F., VAN DER MEIJDE, M., CARRANZA, E.J.M., DE SMETH, J.B. & WOLDAI, T. (2012): Multi- and hyperspectral geologic remote sensing: A review. *International Journal of Applied Earth Observation and Geoinformation* **14**, 112–128.

VORTISCH, W., HARDING, D. & MORGAN, J. (2003): Petrographic analysis using cathodoluminescence microscopy with simultaneous energy-dispersive X-ray spectroscopy. *Mineralogy and Petrology* **79**, 193–202.

WALKER, G., ABUMERE, O.E. & KAMALUDDIN, B. (1989): Luminescence spectroscopy of Mn^{2+} centres in rock-forming carbonates. *Mineralogical Magazine* **53**, 201–211.

WRIGHT, P.J. (1991): A superior cathodoluminescence spectral analysis and imaging system. *Journal de Physique IV* **1** C6, 337–341.

YACOBI, B.G. & HOLT, D.B. (1990): Cathodoluminescence microscopy of inorganic solids, chapter 5.1.2. Cathodoluminescence Detection Systems, 102–106. Plenum Press (New York).

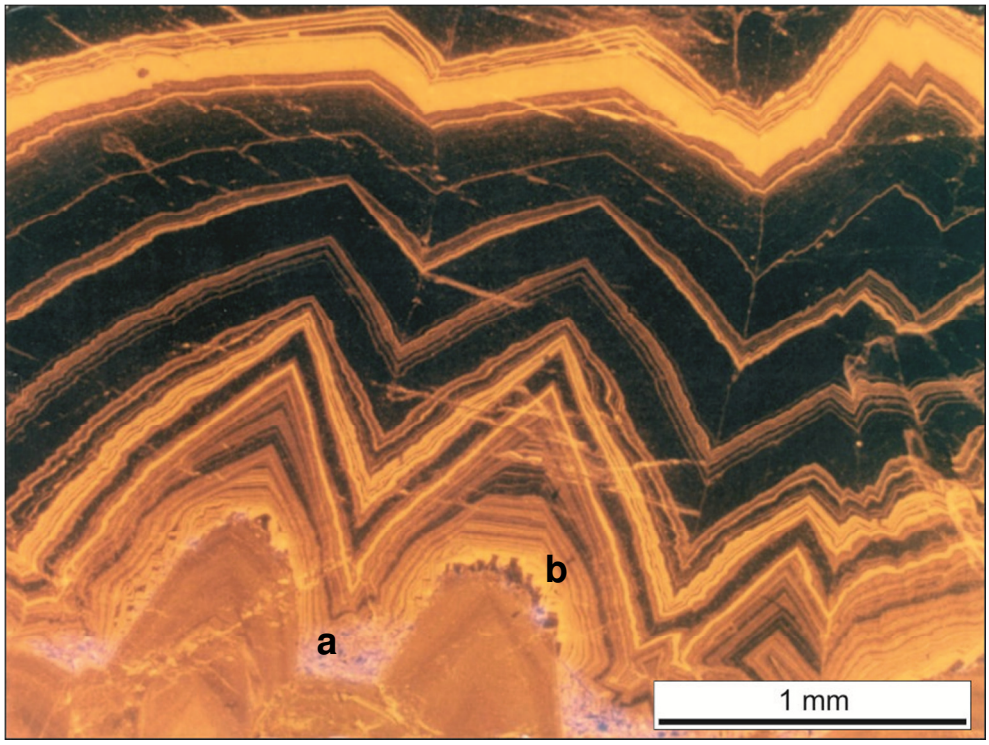

Fig. 1-1. Optical-CL image of zoned calcite cements from the Upper Permian Raisby Formation, north-east England. There are two generations of cement: a lower one with a fairly uniform orange CL, and an upper generation whose narrow orange-luminescent zones decrease in abundance towards the top of the image. During the hiatus between precipitation of the two generations, grains of blue-luminescing fluorite accumulated on the outer surface of the first cement generation.

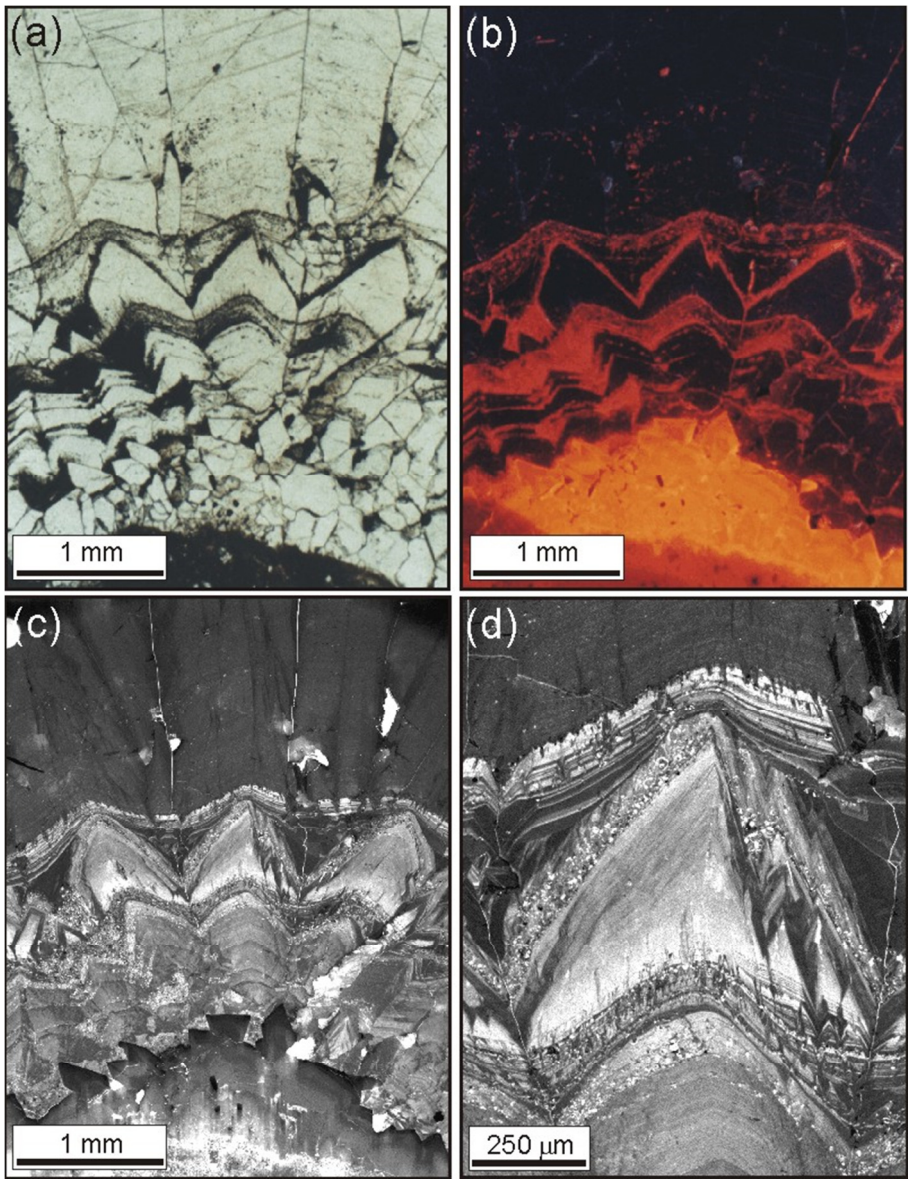

Fig. 1-2. Images of Holocene calcite speleothem from Raisby quarry, County Durham, NE England. (a)–(c) are of the same field of view. (a) Plane polarised transmitted light image showing a sequence of cement layers, each separated by a fine grained internal sediment made mainly of dolomite grains. (b) Optical-CL image showing that only the lowermost part of the cement sequence luminesces at visible wavelengths. The layers of dolomite grains luminesce orange-red. (c) Panchromatic SEM-CL image obtained using an extended dwell time. The orange luminescing calcite has a low CL intensity whereas lower parts of the optically non-luminescent crystals are intricately zoned. (d) Higher magnification panchromatic SEM-CL image of the central part of (c), highlighting the fine detail that can be resolved. Note that although calcite in the upper part of the image is apparently non-luminescent in (c), this image shows that it has a very fine-scale banding.

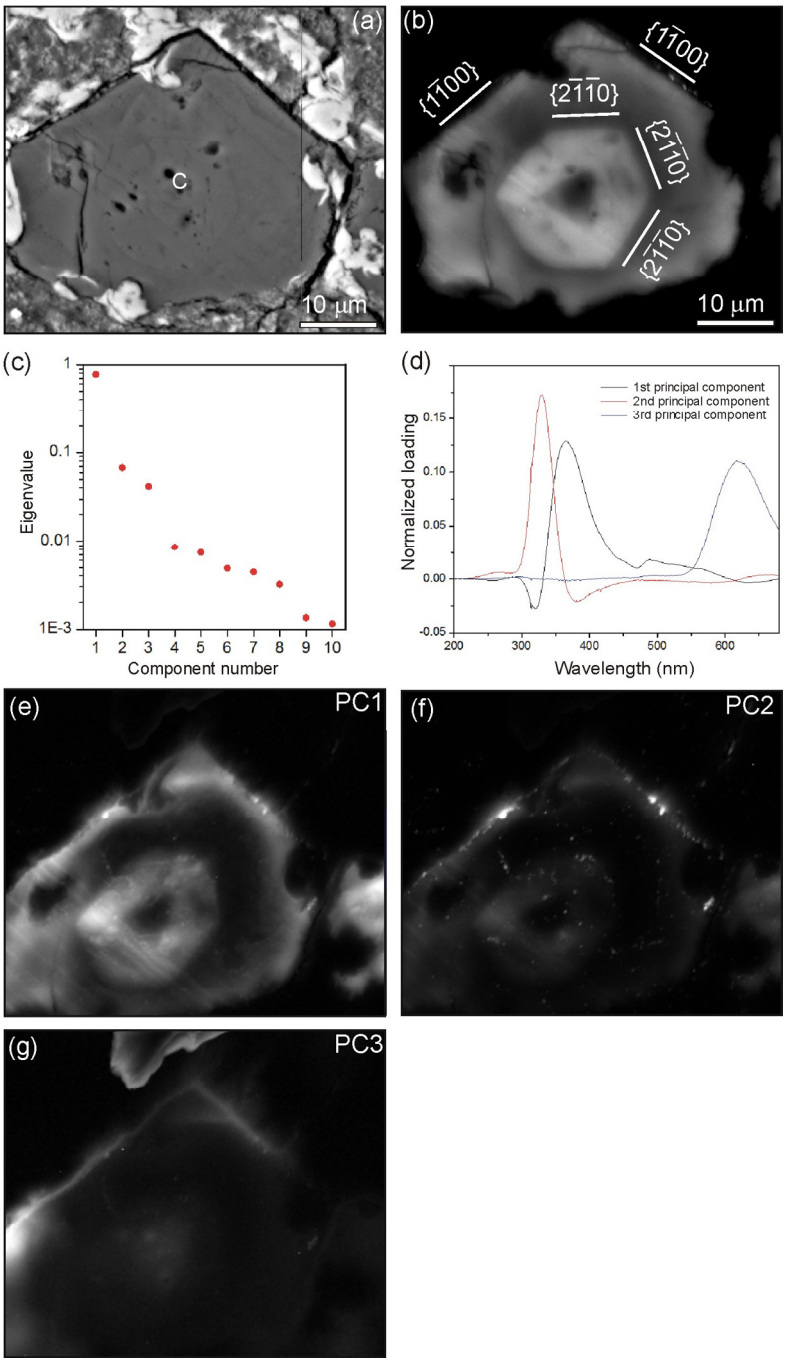

Fig. 1-3. A calcite crystal in the Murray CM2 carbonaceous chondrite meteorite (a) Backscattered electron SEM image of the calcite (C) is enclosed within a matrix containing serpentine-phyllosilicates (mid grey) and a hydrous sulphide called tochilinite (white). (b) Panchromatic SEM-CL image showing that the calcite crystal is zoned, and the crystallographic orientation of zone boundaries, as determined by subsequent EBSD mapping, are indicated. (c) to (g) show the use of principal component in the analysis of CL hyperspectral imaging data, which has been collected from the calcite crystal. The 'scree' plot (c) shows the eigenvalues corresponding to the first 10 principal components: this indicates that around 88% of the variance in the dataset is accounted for by the first 3 components alone. Selecting these three components and applying a varimax rotation yields the spectra shown in (d). The images in (e), (f) and (g) show the relative contribution of these three components at each spatial pixel.

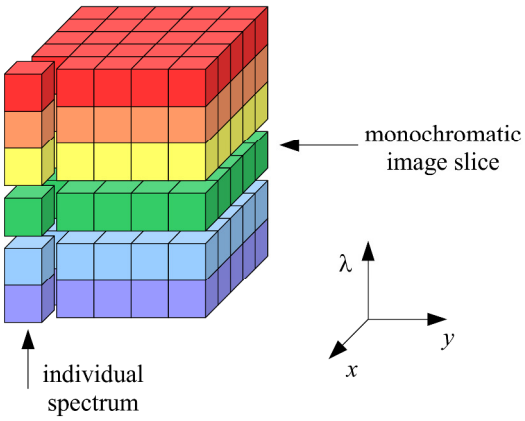

Fig. 1-4. Representation of a hyperspectral image data cube, showing the stack of monochromatic images as horizontal slices and the component spectra as vertical columns.

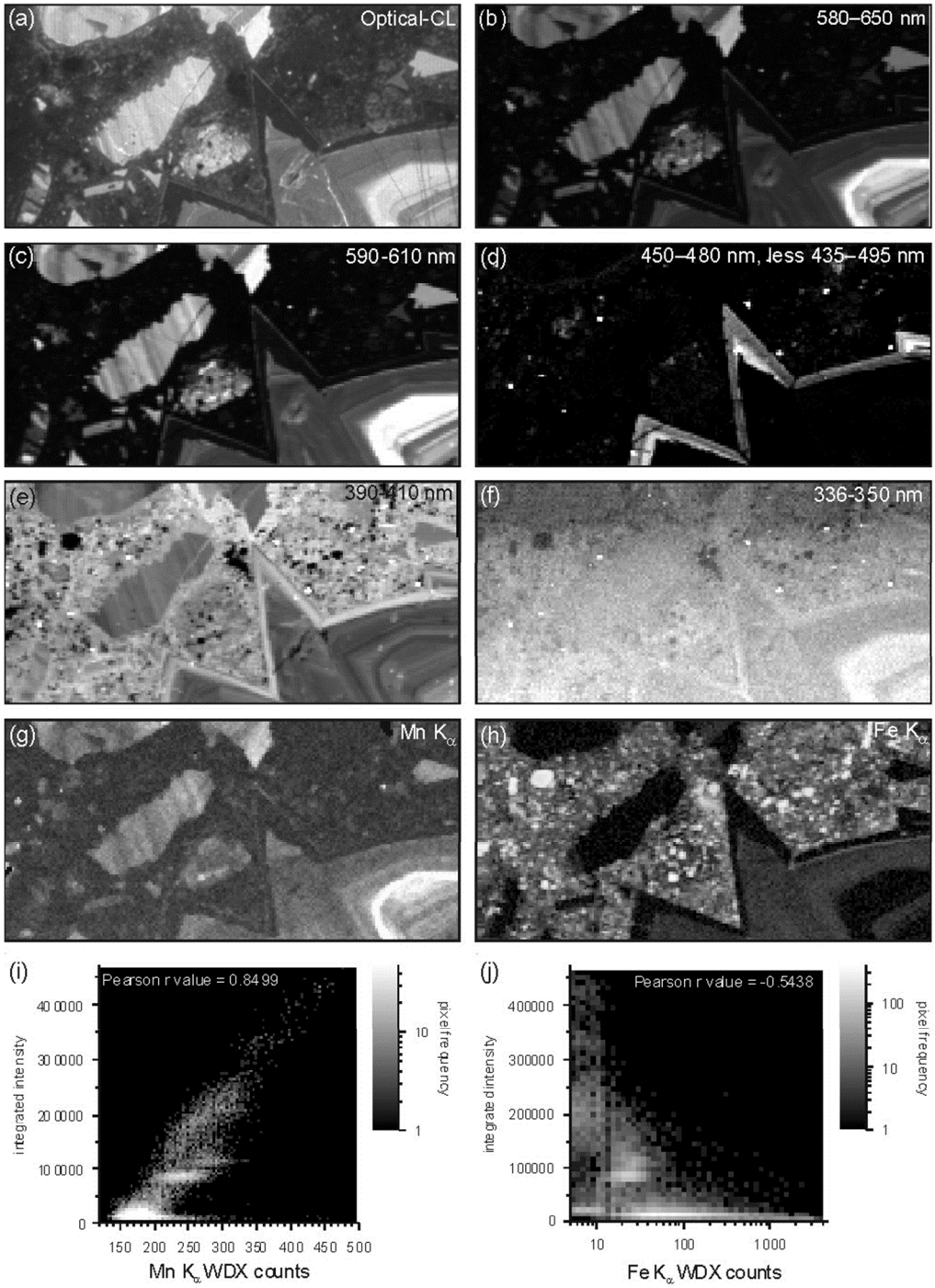

Fig. 1-5. Hyperspectral data from calcite cements of the Upper Permian Raisby Formation, northeast England. Calcite in the lower right hand part of the image is overlain by a dolomite-rich internal sediment that contains calcite fragments. (a) Optical-CL image, (b) to (f) are CL images from different wavelength ranges, as indicated on each image. (b) Intensity range = 0–5×10^6 counts, (c) Intensity range = 0–1×10^5 counts, (d) Intensity range = 0–3×10^3 counts, (e) Intensity range = 0–3×10^4 counts, (f) 0–200 counts. (g) and (f) are WDX maps acquired simultaneously with the CL data (intensity ranges are 120–500 counts and 5–5000 counts (log) respectively). Also shown are correlation plots of the intensity of the 580–650 nm emission band against (i) Mn and (j) Fe WDX counts, generated by plotting the pixel values of map (b) against those from maps (g) and (h) respectively.

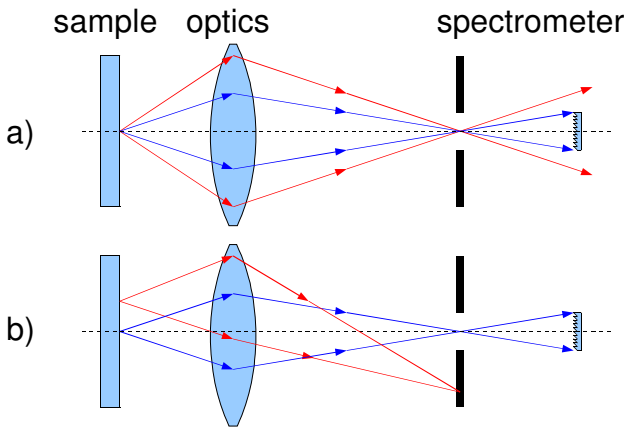

Fig. 1-6. Simplified optical diagrams showing schematically: (a) the loss in signal due to focussing light from a large solid angle into a spectrometer; (b) the limited field of view imposed by forming at image at the entrance slit. These illustrate the trade-off between light collection efficiency, spectral resolution (i.e. slit width) and field of view, which is imposed by the concept of optical étendue.

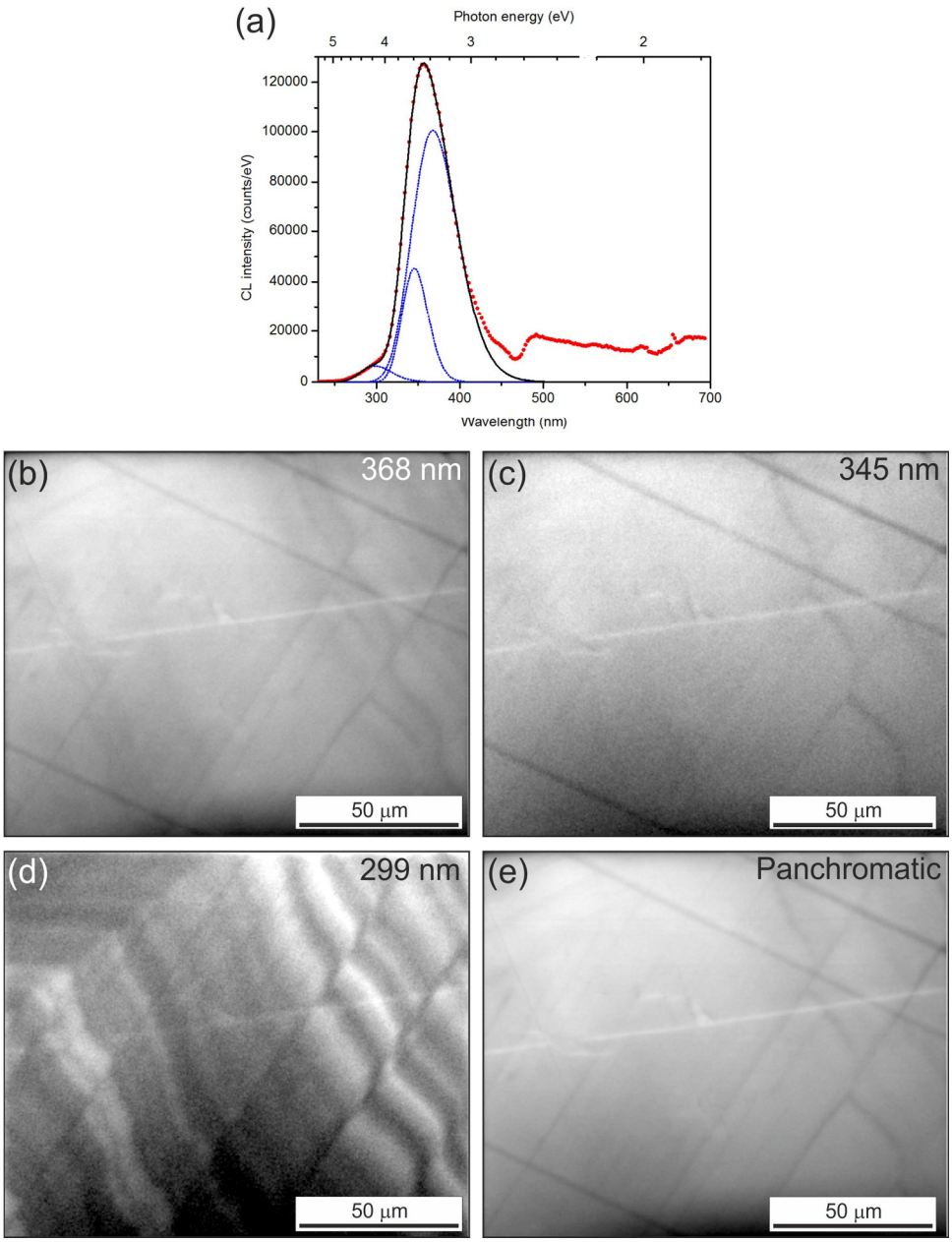

Fig. 1-7. Data from a Holocene calcite speleothem from Raisby quarry, County Durham, NE England (the same sample as in Fig. 1-2), which provides an example of extracting images from a CL hyperspectral fitting using nonlinear least-squares peak fitting. The data points show the mean spectrum calculated from the entire image.The solid line shows the result of fitting three Gaussian peaks to this mean, fitted in the energy regime and over the interval 3–5 eV (248–413 nm). The three component peaks are shown individually using dotted lines. The images show the result of fitting the intensity of these peaks to each spatial pixel in the HSI, while keeping the peak energy and FWHM fixed: (b) 3.37 eV (368 nm), (c) 3.59 eV (345 nm) and (d) 4.15 (299 nm). In terms of CL activators, the longer wavelength bands are probably attributable to an intrinsic (defect) centre whereas the 299 nm map reveals a very fine-scale zoning that suggests an extrinsic centre, possibly Ce^{3+}. Note that this zoning would not be detectable in the panchromatic image (e), so that the hyperspectral technique is crucial for identifying the zoning. The orthogonal straight lines are twin composition planes.